

Manipulating the anisotropic phase separation in strained VO₂ epitaxial films by nanoscale ion-implantation

Changlong Hu¹⁺, Liang Li¹⁺, Xiaolei Wen², Yuliang Chen¹, Bowen Li¹, Hui Ren¹,
Shanguang Zhao¹, Chongwen Zou^{1*}

*¹National Synchrotron Radiation Laboratory, University of Science and Technology of
China, Hefei, 230029, China*

*² Center for Micro- and Nanoscale Research and Fabrication, University of Science
and Technology of China*

Corresponding Author: czou@ustc.edu.cn

+These two authors contributed equally to this paper.

ABSTRACT

Manipulating the strain induced poly-domains and phase transition in correlated oxide material are important for high performance devices fabrication. Though the electronic transport in the strained oxide film at macroscopic scales can be directly measured, the anisotropic electronic state and the controllable phase separation cross the insulator-to-metal transition within nanoscale size are still elusive. Here, we selected VO₂ crystal film as a prototypical oxide and achieved the manipulation of anisotropy electronic phase separation via injecting He⁺ nanobeam into VO₂ film at room temperature. In addition, this nanoscale phase separation was directly visualized by infrared near-field imaging measurements, showing the pronounced and unique c_R-axis dependent anisotropy on VO₂ surface. Our results offered new insights towards understanding the anisotropic nanoscale phase separation in strained metal oxide films.

Correlated oxides have attracted tremendous attention due to the distinct emergent phenomena including the colossal magnetoresistance, insulator-metal transition and high-temperature superconductivity¹, which are closely associated with the degrees of freedom including the spin-charge-lattice-orbital interactions². Specifically, the lattice strains are of particular tool owing to the characteristic that it can cause conspicuous new physics in materials. For example, strain can lower the correlated oxides transition temperature³, the increase of the superconducting critical temperature⁴, the enhancement of the ferroelectric polarization⁵ or even producing giant pseudomagnetic fields⁶. Spontaneous formation of multi-domains by external compressive strain can produce many new macroscopic orders⁷, leading to the coexistence of multiple constituent phases or pronounced phase separations in correlated materials⁸.

As a typical correlated transition metal oxide, vanadium dioxide (VO₂), has attracted tremendous interest due to its special metal-insulator transition (MIT) near the room temperature (~340K)⁹. During the MIT process, VO₂ crystal will change from a low temperature monoclinic (*M*) structure to high temperature rutile (*R*) structure and

the resistance will show a sharp drop with the magnitude of up to five orders¹⁰. It is also revealed that the V^{4+} ions dimers will tilt with respect to the tetragonal c_R axis across the MIT, causing the specimen to expand by 1% along the c_R axis¹¹. Thus the phase transition of VO_2 crystal exhibits pronounced responses to strain stimuli, which always induces multiple phases domains or pronounced phase separations^{12,33}. It is known that manipulate the macroscopic order or control the phase separations is technologically important for VO_2 device fabrication. While till now almost all of the previous studies are focusing on the observations of phase separations triggered by fixed interfacial strain in epitaxial film^{12, 16, 17}, the artificial manipulation of strain to control the phase transition in VO_2 crystal is rarely reported.

In the current study, we prepared VO_2 crystal film by an rf-plasma assisted oxide molecule beam epitaxy (OMBE) on TiO_2 (110) and (001) crystal substrates, respectively. By injecting He^+ nanobeam into VO_2 film, the local strain distribution around the injection zone can be manipulated, which leads to anisotropic phase separations. Moreover, these naonscale anisotropic phase separations can be directly observed by scattering-type scanning near-field optical microscope (s-SNOM) and the anisotropic features strongly dependent on the growth orientation. Combined with the strain simulation results, it is suggested that this anisotropic phase separation mainly due to the local strain field modulated by He^+ nanobeam injection, which is closely associated with the in-plane c_R axis of VO_2 . Our current studies not only reveal the relationship between the anisotropic phase separation and the c_R axis of VO_2 , but also demonstrate a strain manipulation strategy to engineer the phase transition in transition metal oxide.

In this work, epitaxial VO_2 crystal film with the thickness of about 20nm were prepared by an rf-plasma assisted oxide molecule beam epitaxy (OMBE) on TiO_2 (110) and (001) crystal substrates, respectively. Before the deposition, the TiO_2 substrates were ultrasonically cleaned in acetone and alcohol, and then rinsed in deionized water. Finally, the substrates were blown dry by nitrogen gas before introducing into the growth chamber with a base pressure better than 3×10^{-9} Torr. The growth rate was calibrated by quartz crystal microbalance and the growth process was monitored by

reflection high-energy electron diffraction.

The crystal structure of VO₂ epitaxial films were characterized by X-ray diffraction (XRD, Model D/Max 2550 V, Rigaku, Japan) with Cu K α radiation ($\lambda=1.54178\text{\AA}$). The atomic force microscopy (AFM, Dimension Icon from BRUKER) was measured in air at room temperature. The temperature dependent resistance tests for the prepared samples were conducted by a home-made four-probe station with controllable temperature stage. He⁺ Microscopy (HIM, from ZEISS Co.) was applied to inject He⁺ in thin films with the dose of 1500 ions/nm² at 30kV. The infrared nano-imaging was recorded by scattering-type scanning near-field optical microscope (s-SNOM, from Neaspec GmbH Co.). The 10.632 μm Mid-IR was used as the near-field illumination source laser, a homemade constant heater was linked to the s-SNOM.

The commercial software, COMSOL Multiphysics, was used to simulate the distribution of the phases and surface strain along the c axis of the VO₂ films. The 2-dimensional (2D) models of single layer VO₂ films with round (radius = 0.7 μm) and square (side length = 1.4 μm) He⁺ injected areas were built based on a large pristine film (radius = 50 μm) with a round fixed constraint boundary. Meanwhile, the physical module of Structural Mechanics (Solid Mechanics) was applied to calculate the results.

To prepared high-oriented VO₂ film, TiO₂(001) and TiO₂ (110) crystal substrates were used for the film growth. Due to the close crystal lattice parameters for rutile TiO₂ (a=0.459 nm and c=0.296 nm) and rutile VO₂ (a=0.455, and c=0.285 nm), epitaxial VO₂ film can be well-grown by oxide molecular beam epitaxy technique (oxide MBE). Considering the growth facets as shown in Fig.1a and Fig.1d, the c_R axis of the grown VO₂(001)/TiO₂(001) is out of plane, while the c_R axis is in-plane for TiO₂ (110) substrate. The crystal structures were characterized by X-ray diffraction as shown in Fig.1b and 1e. The diffraction peaks at 62.74 and 65.30 ° in Fig.1b are indexed to TiO₂ (002) and VO₂ (002) planes, respectively. No other peaks were shown by XRD analysis, indicating that the prepared film grown by oxide MBE is an (001)-oriented phase. In Fig.1e, the XRD patterns show sharp peaks at 27.44 related to the TiO₂ (110) and the peak at 27.68 is associated with the VO₂ (110)_R.

The temperature dependent resistance measurements for the prepared films were also conducted. In Fig 1c, sharp resistance change up to three-order of magnitude across the metal-insulator transition can be observed for VO₂ (001)/TiO₂ (001) film. While it should be noticed that the critical temperature was ~55°C and obviously lower than that of bulk VO₂ (~68°C). In Fig.1f, the R-T curve is also plotted for VO₂ (110)/TiO₂ (110) film, which shows quite broad hysteresis loop and the increased critical temperature. It was reasonable if considering the interfacial strain/stress from the substrate in epitaxial VO₂/TiO₂ system. The c_R axis is compressed in VO₂(001)/TiO₂(001) film, while stretched in VO₂(110)/TiO₂(110), which resulting the different modulations of the phase transition temperature¹³. This different changes of the critical transition temperatures in these two films indicate the delicate correlation with the status of c_R-axis in VO₂ crystal.

After treated by He⁺ nanobeam implantation with a square injection region, the VO₂ (001) /TiO₂ films were characterized by s-SNOM and AFM as showing in Fig.2. The scheme for the s-SNOM technique is shown in Fig.2a, which combines the advantages of phase sensitive of infrared light and the high spatial resolution of probe microscopy. By using the s-SNOM technique, it is clear to observe the phase transition of the VO₂ film sample after He⁺ implantation with different naonbeam sizes in Fig.2b. It is suggested that for s-SNOM test, the detected signal S_n is the light scattered by the tip demodulated at the *n*th harmonic of the tip tapping frequency^{14,15}. Thus we choose S₃, the tip-scattered light demodulated at the third harmonic of the tapping frequency, to obtain the relatively useful signals considering the relationship between background signal and overall signal strength^{15,16}. Fig.2c and 2d show the detailed s-SNOM images for VO₂ (001) sample after He⁺ implantation with the beam size of 2μm × 2μm, while Fig.2e shows the AFM image for the same area. Since higher local optical conductivities yield stronger infrared near-field signal, the s-SNOM image with the bright square reveals that the He⁺ injection area has been transferred from the original insulating to metallic phase. In addition, this phase transition is quite homogenous within the square area after He⁺ injection. In fact, for the current He⁺ radiated VO₂ (001)

sample, we also conducted the temperature dependent resistance measurement (See supplementary FIG.1) for the He⁺ radiated and untreated areas, respectively, which clearly showed the metallic feature and normal phase transition behavior, respectively. This observation is consistent with previous report¹⁷, which demonstrated that Ar⁺ implantation will induce the metallic VO₂ phase at room temperature. It is possible to highlight the degree of correlation between AFM topography and infrared near-field amplitude (S₃) at the same coordinate system as shown in Fig.2f. The line scans of AFM topography (black curve) and the near-field S₃ amplitude (red curve) along the direction by the dotted arrow show almost the same profiles, indicating the unmistakable correlation between the infrared near-filed amplitude and topographic features for VO₂ (001)/ TiO₂ film.

While for VO₂ (110)/ TiO₂ film, the same He⁺ beam treatment with a square region will induce quite different results as shown in Fig. 3. The s-SNOM images in Fig.3a and 3c reveal that the He⁺ injected VO₂ (110) film can produce pronounced phase separations. Perpendicular to the c_R axis direction, two bright stripes appears along two edges of the squared region. Since higher local optical conductivities yield stronger infrared near-field signal, it is suggested that there appears anisotropic metallic stripes caused by the He⁺ flux treatment. The AFM mapping image in Fig.3b shows the clear protuberant square area after the He⁺ implantation, which is similar as the observation for VO₂ (001) film in Fig.2e. The line scans of AFM topography (black curve) and the near-field S₃ amplitude (red curve) along the direction by the dotted arrow for the ion-flux treated VO₂ (110)/ TiO₂ (110) film is also plotted in Fig. 3d. The height variation and the infrared near-filed amplitude is completely not consistent, which indicates different correlation between the two effects if comparing with the VO₂ (001)/ TiO₂ (001) film (Fig. 2f).

In fact, this different correlation depending on the growth orientation can be reproducible, even if changing the He⁺ injection area from square to circle shape (See supplementary Fig.1 and Fig.2). It is interesting to see that the phase separations in the nanoscale range induced by the ion injection in VO₂(110)/TiO₂(110) films with the square shape are two parallel stripes, while two distinct arcs around the injection circle

area shown in Fig.2S. In addition, it is also found that the metallic phase stripes are always perpendicular to the c_R axis direction, showing the distinct anisotropic feature.

From the above results, it is deduced that the c_R axis should play a key role in this nanoscale phase separation for the strained VO₂ film. In addition to the changing optical signal of the injected regions, the height variation can provide important hint about the underlying mechanisms that govern the MIT via strain. For the VO₂(001) /TiO₂ (001) film, the c_R axis is out-of-plane, the He⁺ injection induced phase transition is homogenous and the anisotropic phase separation by ion injection is not observed. While for VO₂(110) /TiO₂ (110) film, the c_R axis is in-plane. Due to the He⁺ insertion, the injected region will swell and form a big bump. Under this condition, the localized VO₂ crystal at the edges perpendicular to the c_R direction will have a compressed c_R value and lead to the metallic phase at the room temperature, which is clearly observed in the SNOM optical signal with anisotropic character in Fig.3 or Supplementary Fig.2. This anisotropic phase separation in nanoscale range can also be clearly observed in Fig.4. In fact, if we inject the He⁺ flux onto VO₂ (110) film with the shape of number “2” or number “3” as shown in Fig.4a or 4c, the edges or arcs which are perpendicular to the c_R axis, all show bright sections, indicating the metallic phase structures induced by the local He⁺ flux treatment. The related 3D profile of the s-SNOM signal in Fig.4b or 4d further confirm the anisotropic features of the local phase separation.

To further explore the c_R axis dependent anisotropic character of the phase separation for VO₂(110) /TiO₂ (110) film, we just change the He⁺ injection square region with a rotate angle (the square bottom edge and c_R direction) from parallel to 45° and 60°, respectively. From Fig.5a~5c, it can be observed that for the initial stage, the two bright stripes are perpendicular to c_R direction (Fig.5a). When rotating the square with 45°, the phase separation is distinct at the two vertex-angle along the c_R direction. While if angle further changes to 60°, the two stripes also tilt to the same angle. These angle-dependent s-SNOM signals clearly confirm the anisotropic phase separation, which can be directly manipulated by adjusting the profile of the He⁺ injection area.

The interfacial strain/stress simulation appears to provide a solid evidence for understanding this anisotropic phase separation in nanoscale. Since the strain distribution is quite closely associated with the phase separation on the film surface, the anisotropic strain distribution mapping as well as the local phase separation can be simulated at the same time (see supplementary Fig.3). Considering the He⁺ injection square area, the simulations of the phase distribution mapping for VO₂/TiO₂(110) film with different orientations referred to the in-plane c_R axis are conducted(see supplementary Fig.4), showing the strong c_R axis dependence. Thus, comparing with the s-SNOM observations in Fig.5a~5c with a rotated square area, the simulations showing in Fig.5d~5f are quite consistent, confirming the anisotropic phase separation in nanoscale induced by the He⁺ injection.

Considering the different symmetry of the He⁺ injection shapes on VO₂/TiO₂(110) film (square or circle), the local the anisotropic strain distribution mapping are also simulated for both cases(see supplementary Fig.5). During the simulation, the anisotropic factors are well considered (see supplementary Note 1). For the circle shape (see supplementary Fig 6), the simulation results show that the increasing of the pressure can only raise the absolute value of the strain rather than affect the distribution of the strain, which directly reflected by the anisotropic phase separations in nanoscale size.

In summary, He⁺ nanobeam injection into VO₂ film will induce homogenous metallic phase transition for VO₂ (001) film, while under the same condition, anisotropic phase separations are observed in nanoscale by s-SNOM in VO₂ (110) film, which show pronounced c_R-axis dependency. Combined with the AFM topography images, it is suggested that the He⁺ implantation induced swelled region plays a key role in the phase separation in VO₂(110)/TiO₂ (110) epitaxial film. Theoretical simulations are quite consistent with the experimental observations, further confirming the phase separation induced by the compressed c_R value in the local area, which can be directly manipulated by adjusting the He⁺ injection profile. The current studies not only reveal the c_R-axis dependent phase separation in VO₂ (110) film, but also provide

an effective strategy to engineer phase transitions in nanoscale level for tuning the properties of correlated oxide system.

This work was partially supported by the National Natural Science Foundation of China (12074356), the Open Research Fund of State Key Laboratory of Pulsed Power Laser Technology and the Youth Innovation Promotion Association CAS. This work was partially carried out at the USTC Center for Micro and Nanoscale Research and Fabrication. The authors also acknowledged the supports from the Anhui Laboratory of Advanced Photon Science and Technology.

DATA AVAILABILITY

The data that support the findings of this study are available from the corresponding authors upon reasonable request.

REFERENCES

- ¹ Elbio Dagotto, Takashi Hotta, and Adriana Moreo, *Physics reports* **344** (1-3), 1 (2001); Vijay B Shenoy, DD Sarma, and CNR Rao, *ChemPhysChem* **7** (10), 2053 (2006); Mb Tinkham, *Physical review letters* **61** (14), 1658 (1988).
- ² DI Khomskii and GA Sawatzky, *Solid state communications* **102** (2-3), 87 (1997); H Kuwahara, Y Moritomo, Y Tomioka, A Asamitsu, M Kasai, R Kumai, and Y Tokura, *Physical Review B* **56** (15), 9386 (1997); Y Tokura and N Nagaosa, *science* **288** (5465), 462 (2000).
- ³ Nagaphani B Aetukuri, Alexander X Gray, Marc Drouard, Matteo Cossale, Li Gao, Alexander H Reid, Roopali Kukreja, Hendrik Ohldag, Catherine A Jenkins, and Elke %J Nature Physics Arenholz, *Nature Physics* **9** (10), 661 (2013); LL Fan, S Chen, ZL Luo, QH Liu, YF Wu, L Song, DX Ji, P Wang, WS Chu, and C Gao, *Nano letters* **14** (7), 4036 (2014).
- ⁴ J-P Locquet, J Perret, J Fompeyrine, E Mächler, Jin Won Seo, and G Van Tendeloo, *Nature* **394** (6692), 453 (1998).
- ⁵ JBNJ Wang, JB Neaton, H Zheng, V Nagarajan, SB Ogale, B Liu, D Viehland, V Vaithyanathan, DG Schlom, and UV Waghmare, *science* **299** (5613), 1719 (2003).
- ⁶ N Levy, SA Burke, KL Meaker, M Panlasigui, A Zettl, F Guinea, AH Castro Neto, and Michael F Crommie, *Science* **329** (5991), 544 (2010).
- ⁷ MK Liu, M Wagner, E Abreu, S Kittiwatanakul, A McLeod, Z Fei, M Goldflam, S Dai, MM Fogler, and J Lu, *Physical review letters* **111** (9), 096602 (2013); Vera Lyahovitskaya, Yishay Feldman, Ilya Zon, Ellen Wachtel, Igor Lubomirsky, and AL Roytburd, *Advanced Materials* **17** (16), 1956

- (2005); RJ Zeches, MD Rossell, JX Zhang, AJ Hatt, Q He, C-H Yang, A Kumar, CH Wang, A Melville, and C Adamo, *science* **326** (5955), 977 (2009).
- ⁸ KH Ahn, T Lookman, and AR Bishop, *Nature* **428** (6981), 401 (2004); Thomas Z Ward, John D Budai, Zheng Gai, Jonathan Zachary Tischler, Lifeng Yin, and Jian Shen, *Nature Physics* **5** (12), 885 (2009).
- ⁹ Shi Chen, Zhaowu Wang, Hui Ren, Yuliang Chen, Wensheng Yan, Chengming Wang, Bowen Li, Jun Jiang, and Chongwen Zou, *Science advances* **5** (3), eaav6815 (2019); Javier Del Valle, Pavel Salev, Federico Tesler, Nicolás M Vargas, Yoav Kalcheim, Paul Wang, Juan Trastoy, Min-Han Lee, George Kassabian, and Juan Gabriel Ramírez, *Nature* **569** (7756), 388 (2019); Tom Driscoll, Hyun-Tak Kim, Byung-Gyu Chae, Bong-Jun Kim, Yong-Wook Lee, N Marie Jokerst, Sabarni Palit, David R Smith, Massimiliano Di Ventra, and Dimitri N Basov, *Science* **325** (5947), 1518 (2009).
- ¹⁰ Maurits W Haverkort, Z Hu, Arata Tanaka, W Reichelt, SV Streltsov, MA Korotin, VI Anisimov, HH Hsieh, H-J Lin, and CT Chen, *Physical review letters* **95** (19), 196404 (2005); TC Koethe, Z Hu, MW Haverkort, C Schüßler-Langeheine, F Venturini, NB Brookes, Oscar Tjernberg, W Reichelt, HH Hsieh, and H-J Lin, *Physical review letters* **97** (11), 116402 (2006); Zhensheng Tao, Tzong-Ru T Han, Subhendra D Mahanti, Phillip M Duxbury, Fei Yuan, Chong-Yu Ruan, Kevin Wang, and Junqiao Wu, *Physical review letters* **109** (16), 166406 (2012).
- ¹¹ Elsa Abreu, Mengkun Liu, Jiwei Lu, Kevin G West, Salinporn Kittiwatanakul, Wenjing Yin, Stuart A Wolf, and Richard D Averitt, *New Journal of Physics* **14** (8), 083026 (2012); JC Rakotoniaina, R Mokrani-Tamellin, JR Gavarrri, G Vacquier, A Casalot, and G Calvarin, *Journal of Solid State Chemistry* **103** (1), 81 (1993).
- ¹² Bence Lazarovits, Kyoo Kim, Kristjan Haule, and Gabriel Kotliar, *Physical Review B* **81** (11), 115117 (2010).
- ¹³ S. Chen, L. L. Fan, J. Wang, Y. Pan, F. H. Chen, P. S. Xu, C. W. Zou, and Z. Y. Wu, *Surface and Coatings Technology* **258**, 1196 (2014).
- ¹⁴ A Cvitkovic, N Ocelic, and R Hillenbrand, *Nano letters* **7** (10), 3177 (2007).
- ¹⁵ Lukas Novotny and Bert Hecht, *Principles of nano-optics*. (Cambridge university press, 2012).
- ¹⁶ Lena Jung, Thomas Taubner, and Thomas Schäpers, 2020.
- ¹⁷ Jura Rensberg, Shuyan Zhang, You Zhou, Alexander S McLeod, Christian Schwarz, Michael Goldflam, Mengkun Liu, Jochen Kerbusch, Ronny Nawrodt, and Shriram Ramanathan, *Nano letters* **16** (2), 1050 (2016).

Figures and Captions

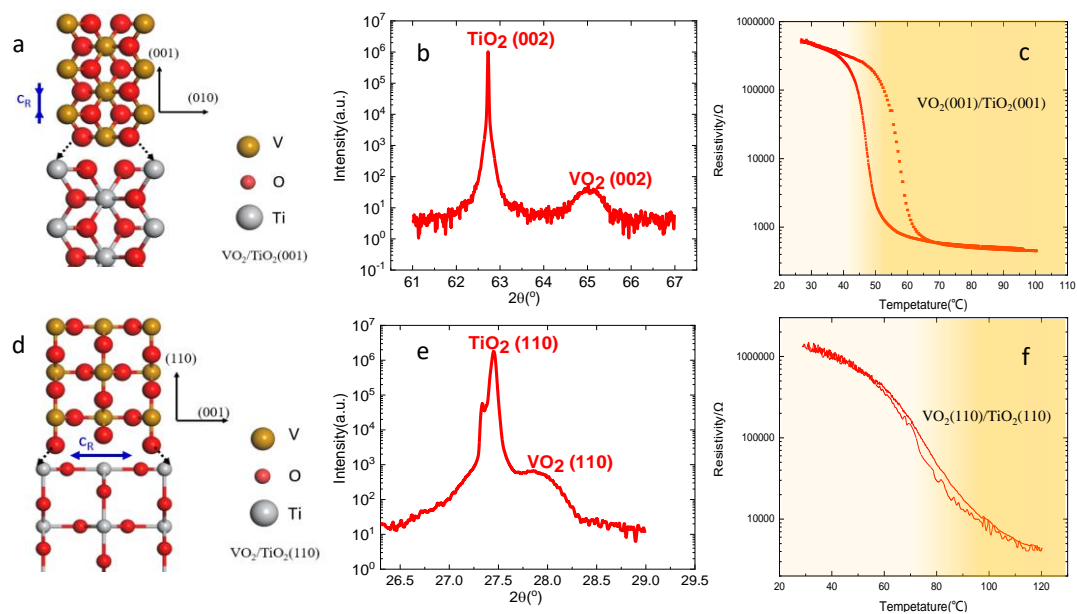


FIG. 1. Characterizations for the prepared VO₂ film. (a) Scheme for the epitaxial VO₂ (001) film grown on TiO₂ (001) crystal substrate; (b, c) The XRD and R-T curves for VO₂ (001) film. The phase transition temperature is lower than that of bulk due to the interfacial stress induced shrink c_R axis; (d) Scheme for the epitaxial VO₂ (110) film grown on TiO₂ (110) crystal substrate; (e, f) The XRD and R-T curves for VO₂ (110) film. The phase transition temperature is higher than that of bulk due to the interfacial stress induced expand c_R axis.

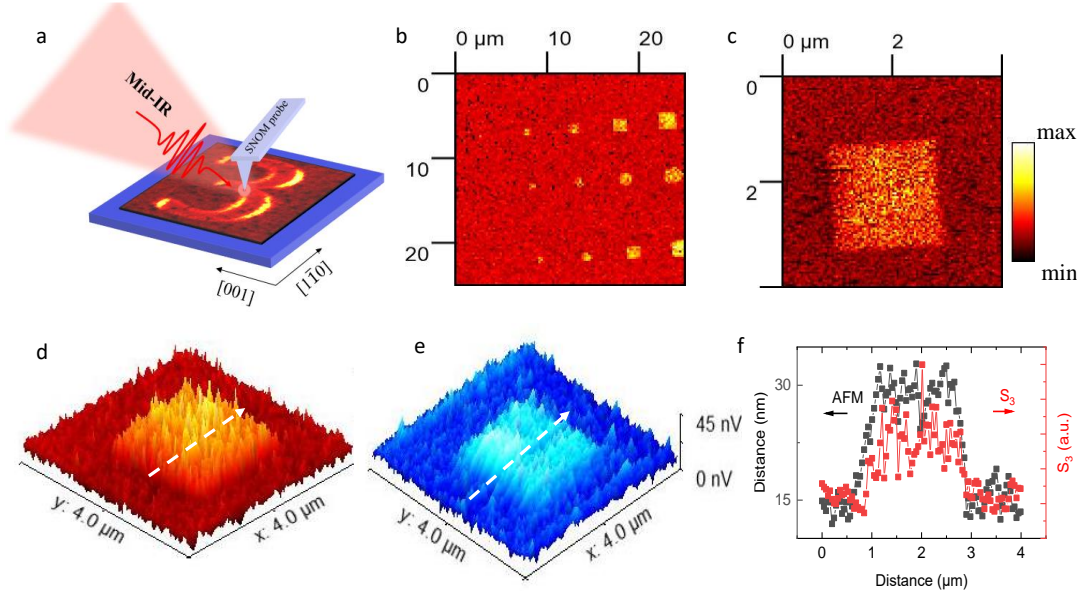


FIG. 2. The s-SNOM test for VO_2 (001)/ TiO_2 film after He^+ implantation. (a) The scheme for the s-SNOM technique; (b) The s-SNOM image (scattering amplitude S_3 mapping) for the sample after He^+ implantation with different beam sizes. (c) The s-SNOM image for the sample after He^+ insertion with the size of $2\mu\text{m} \times 2\mu\text{m}$, showing a homogenous metallic state in the whole square area; (d) The 3D scattering amplitude S_3 image and (e) the 3D-AFM topography image for the film after He^+ insertion with the size of $2\mu\text{m} \times 2\mu\text{m}$; (f) The line scans of AFM topography (black curve) and the near-field S_3 amplitude (red curve) along the dotted arrow lines in (d) and (e).

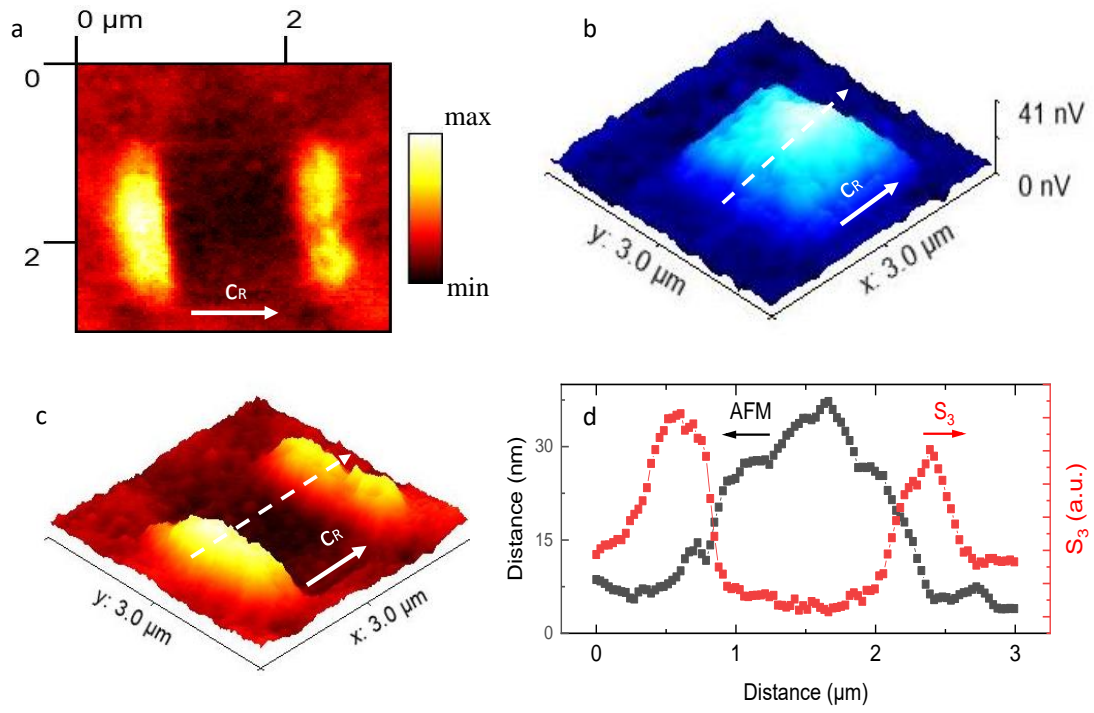


FIG. 3. The s-SNOM test for $\text{VO}_2(110)/\text{TiO}_2$ film after He^+ implantation. (a) The s-SNOM image (scattering amplitude S_3 mapping) for the sample after He^+ insertion, showing two stripe-like metallic phases perpendicular to c_R -axis; (b) The 3D-AFM topography image and (c) the 3D scattering amplitude S_3 image for the film after after He^+ insertion; (d) The line scans of AFM topography (black curve) and the near-field S_3 amplitude (red curve) along the dotted arrow lines in (b) and (c).

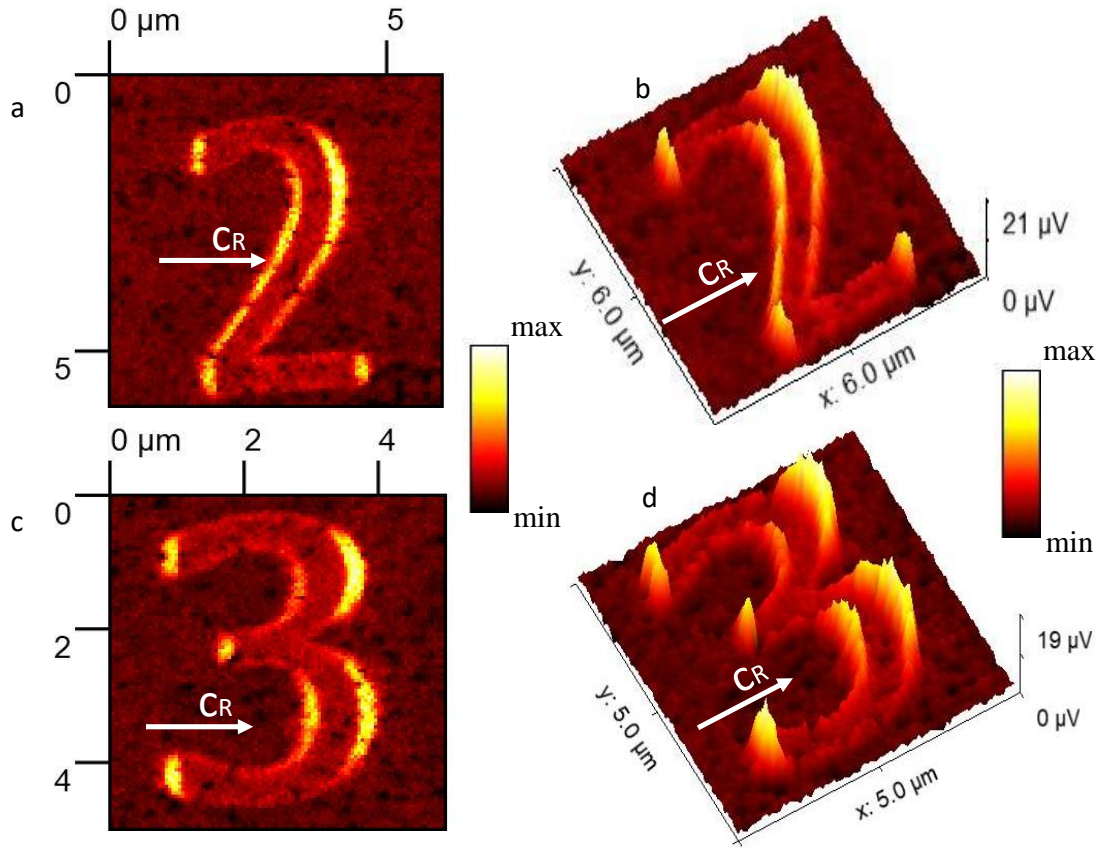


FIG.4. The s-SNOM image (scattering amplitude S3 mapping) for the VO₂ grown TiO₂(110) after He⁺ insertion with circle area with the shape of number “2” (a) and number “3” (c), the (b) and (d) representing the 3D scattering amplitude S3 image of (a) and (c), respectively.

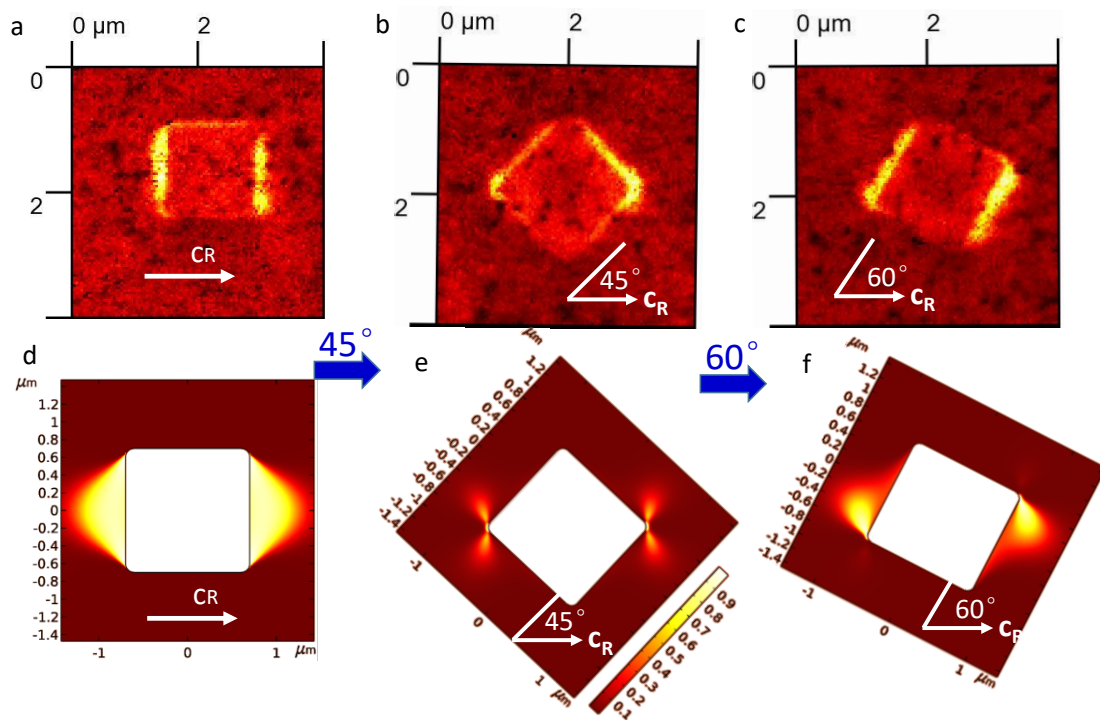


FIG.5. Experimental and Simulations for the anisotropic phase separation. (a~c) The s-SNOM images (scattering amplitude S_3 mapping) for the sample after He^+ insertion by changing the angle between the square bottom edge and c_R direction; (d~f) The simulations for the anisotropic phase separation depending on c_R axis direction, consistent with the s-SNOM observations for the anisotropic phase separation.